

Substrate screening effects on the quasiparticle band gap and defect charge transition levels in MoS₂

Mit H. Naik and Manish Jain

Center for Condensed Matter Theory, Department of Physics, Indian Institute of Science, Bangalore 560012, India

(Received 9 November 2017; published 8 August 2018)

Monolayer MoS₂ has emerged as an interesting material for nanoelectronic and optoelectronic devices. The effect of substrate screening and defects on the electronic structure of MoS₂ are important considerations in the design of such devices. We find a giant renormalization to the free-standing quasiparticle band gap in the presence of metallic substrates, in agreement with recent scanning tunneling spectroscopy and photoluminescence experiments. Our sulfur vacancy defect calculations using the density functional theory plus *GW* formalism, reveal two charge transition levels (CTLs) in the pristine band gap of MoS₂. The (0/−1) CTL is significantly renormalized with the choice of substrate, with respect to the pristine valence band maximum (VBM). The (+1/0) level, on the other hand, is pinned 100 meV above the pristine VBM for the different substrates. This opens up a pathway to effectively engineer defect charge transition levels in two-dimensional materials through the choice of substrate.

DOI: [10.1103/PhysRevMaterials.2.084002](https://doi.org/10.1103/PhysRevMaterials.2.084002)

I. INTRODUCTION

MoS₂, part of the family of layered transition-metal dichalcogenides (TMDCs), has garnered great interest owing to its diverse applications in nanoelectronics and optoelectronics [1–3]. High current on-off ratios in field-effect transistors as well as efficient valley and spin control with optical helicity have been achieved using MoS₂ [4,5]. The direct band gap in monolayer MoS₂ is exploited in building ultrasensitive phototransistors [6–8]. MoS₂ is also considered a promising alternative to platinum as a catalyst in the hydrogen evolution reaction [9–11].

The effect of the dielectric environment and defects on the electronic structure of MoS₂ are the most important considerations in the design of devices using MoS₂ [12–15]. Single-layer MoS₂, achieved through transfer postexfoliation or through direct epitaxial growth [13,16], is typically supported on a substrate [16–20]. Scanning tunneling spectroscopy (STS) measures the quasiparticle band gap of MoS₂ on metallic substrates [16,21]. The screening from the metal is consistently found to reduce the gap [13,16,21–23]. In the presence of graphene or graphite as a substrate, a renormalization larger than 300 meV is observed in the quasiparticle band gap of MoS₂ [13,16,23–27]. Photoluminescence properties of MoS₂ are also strongly influenced by the ambient dielectric environment [16,28]. A redshift in exciton peaks due to substrate screening effects is computed in Ref. [29].

The most abundant native defect found in monolayer MoS₂ is the sulfur vacancy [12]. Sulfur vacancies induce states in the gap of pristine MoS₂, thus affecting its electronic and optical properties [9,30,31]. Noise nanospectroscopy to probe the ionization dynamics of sulfur vacancy defects in MoS₂ shows 0 and −1 charge states of the defect to be stable [32]. Charged-impurity scattering from sulfur vacancies could thus be an important factor limiting the mobility of carriers in MoS₂ [32]. While effort is constantly being made at attaining a lower concentration of defects in MoS₂, sulfur vacancies have found a favorable role in enhancing the rate of the hydrogen evolution

reaction [9]. Defect levels induced by sulfur vacancies in the band gap are responsible for the adsorption of hydrogen [9,33]. The strength of hydrogen binding at the defect sites is determined by the difference in energy between the defect state and the Fermi level [33]. This binding is favorable for catalysis if the hydrogen is bound neither too strongly nor too weakly [34]. Pathways to engineer the position of the defect level in the gap are thus vital to enhance the hydrogen evolution reaction [9,35].

A number of theoretical calculations, based on first-principles density functional theory (DFT) [36,37], have been carried out to study sulfur vacancies in monolayer MoS₂ [30,38–42]. The calculation of charged defects and in turn the charge transition levels (CTLs) within DFT has pitfalls owing to the underestimation of the band gap in the Kohn-Sham DFT [43]. Some simulations use hybrid functionals, as proposed by Heyd, Scuseria, and Ernzerhof (HSE) [44], as an attempt to overcome the band-gap problem [30,38]. However, the band gap of monolayer MoS₂ computed using HSE is about 2.2 eV [30,38,45,46], which is 0.5 eV smaller than the experimentally measured quasiparticle band gap of free-standing MoS₂ [47]. This could affect the results on the defect CTLs in MoS₂. Furthermore, substrate screening effects cannot be effectively studied using DFT or hybrid functionals [48].

Many-body perturbation theory in the *GW* approximation has been combined with DFT in the well-known DFT+*GW* formalism [49,50] and has been used to predict accurate defect formation energies and CTLs [51–53]. In the DFT+*GW* formalism, the energy associated with atomic relaxations on adding an electron is taken into account at the DFT level, and the quasiparticle excitation energy at the *GW* level. Performing *GW* calculations on transition-metal dichalcogenides (TMDCs) in particular are computationally challenging owing to the stringent convergence parameters [54–56]. A DFT+*GW* study on defects in TMDCs, which entails supercell calculations, requires a massive computation. Additionally, the effect of substrate screening can be taken into account accurately within the *GW* approximation [48,55,57,58]. While it is known

that metallic substrates significantly renormalize the pristine quasiparticle band gap, it is not apparent if the defect levels will continue to prevail in the pristine gap or be pushed above or below the pristine conduction band minimum (CBM) or valence band maximum (VBM), respectively.

In this paper, we study the effect of substrate screening on the quasiparticle band gap and defect charge transition levels in monolayer MoS₂. We have considered graphene, hexagonal BN, graphite, and SiO₂ as substrates. At the DFT level, we find that these substrates do not influence the electronic structure of MoS₂. This is due to the absence of long-range correlation effects in DFT. At the *GW* level, however, we find a significant renormalization in the quasiparticle band gap in the presence of these substrates. The quasiparticle gap is renormalized from its free-standing value of 2.7 to 2.4 eV in the presence of graphene and to 2.2 eV in the presence of graphite as the substrate. In the presence of BN or SiO₂, the gap is close to that of free-standing MoS₂. These results are in good agreement with recent experimental measurements [13,16,21,47,59–62]. We also study the electronic structure of MoS₂ in the presence of sulfur vacancy defects. The sulfur vacancy induces states in the pristine band gap of MoS₂. We compute the CTLs of the sulfur vacancy using the DFT+*GW* formalism. Two CTLs appear in the quasiparticle gap: The (+1/0) and (0/−1) levels are 0.1 and 2.2 eV above the pristine VBM, respectively. We further study the effect of substrate screening on the CTLs. The (+1/0) level lies within 100 meV of the VBM in the presence of substrates as well. The (0/−1) level, on the other hand, is significantly renormalized and can be tuned with the choice of substrate.

II. COMPUTATION DETAILS

The density functional theory (DFT) calculations are performed using the plane-wave pseudopotential package QUANTUM ESPRESSO [63]. We use the local density approximation for the exchange correlation functional and norm-conserving pseudopotentials. The wave functions are expanded in plane waves up to an energy cutoff of 250 Ry. For the unit cell MoS₂ calculations, the cell dimension in the out-of-plane direction is fixed at 35 Å and the Brillouin zone sampled with a $12 \times 12 \times 1$ *k*-point grid. The relaxed in-plane lattice parameter of MoS₂ is 3.15 Å. We simulate a sulfur vacancy in MoS₂ by constructing a 5×5 in-plane supercell and removing a sulfur atom. The cell dimension in the out-of-plane direction here is fixed at 18 Å. A *k*-point sampling of $2 \times 2 \times 1$ is used in the supercell calculations. The formation energy of charged sulfur vacancies computed at the DFT level need to be corrected for the spurious electrostatic interaction between the charge and its periodic images. The electrostatic corrections are computed using the COFFEE code [64].

The quasiparticle excitation energies are computed using the BERKELEYGW code [65–67]. For the unit cell MoS₂ calculation, we use a *k*-point sampling of $24 \times 24 \times 1$ and 8400 valence and conduction states. We find the quasiparticle band gap of monolayer MoS₂ to be 2.7 eV, which is in good agreement with previous calculations and experimental measurements [24,47,54,68]. For the supercell calculations, we use a *k*-point sampling of $2 \times 2 \times 1$ and 19 000 valence and conduction states. We find that these parameters are sufficient

TABLE I. Convergence of the band gap as a function of Brillouin zone (BZ) sampling and number of bands.

BZ sampling	$24 \times 24 \times 1$	$12 \times 12 \times 1$	$12 \times 12 \times 1$	$10 \times 10 \times 1$
N_b	6000	6000	750	750
Gap at <i>K</i> (eV)	2.74	2.79	2.78	2.85
Gap at Γ (eV)	4.02	4.06	4.08	4.13

to converge the gap at the *K* point in the Brillouin zone to within 0.2 eV (see Table I). The first 9000 lowest-energy wave functions are treated using a plane-wave energy cutoff of 150 Ry, and the rest of the 10 000 wave functions are treated using a smaller cutoff of 50 Ry. We find that this method produces accurate results at a significantly reduced computation time. The states with low energy, below the Fermi level, are spatially localized. These gradually become more plane-wave-like at higher energies. The higher-energy wave functions can thus be described with a fewer number of plane waves. We have tested this method using the unit cell MoS₂. We find that the *GW* band gap is unchanged if we use the first 60 wave functions at a 150-Ry cutoff and the rest at a 50-Ry cutoff. It is worthwhile to note that the wave functions generated with the 50-Ry cutoff need to be orthonormalized to the 150-Ry cutoff wave functions. This is done in the following manner for the defect supercell calculations. We first generate 9000 lowest-energy wave functions at an energy cutoff of 150 Ry. We then generate 19 000 lowest-energy wave functions with an energy cutoff of 50 Ry. We compute the overlap of these 19 000 with the original 9000 bands. The bands with a large overlap with the original wave functions are left out, and the remaining are orthonormalized with the original [69]. We use PRIMME [70,71] to generate the 9000 bands at 150-Ry cutoff and SCALAPACK [72] exact diagonalization routines to generate the 19 000, 50-Ry cutoff wave functions. Further, the static remainder technique [73] is used to accelerate the convergence of the calculation with the number of empty states. A dielectric cutoff of 35 Ry is used. The Coulomb interaction along the out-of-plane direction is truncated for the computation of the dielectric matrix and self-energy [74]. The dielectric function is extended to finite frequencies using the Hybertsen-Louie generalized plasmon pole (GPP) model [67].

The substrates included in our calculations are BN, SiO₂, graphene, bilayer graphene (BLG), trilayer graphene (TLG), and graphite. The wave-function cutoff used is 70 Ry for BN and SiO₂, and 60 Ry for graphene, BLG, TLG, and graphite calculations. The *k*-point sampling used for graphene, BLG, and TLG is $21 \times 21 \times 1$. The *k*-point sampling used for graphite is $21 \times 21 \times 10$. The *k*-point sampling used for BN and SiO₂ is $15 \times 15 \times 1$ and $14 \times 14 \times 14$, respectively. For the two-dimensional (2D) substrates, the cell dimension in the out-of-plane direction is chosen to match that of MoS₂. We use the semiempirical Grimme [75] scheme to account for the van der Waals interactions between the layers in heterostructures constructed at the DFT level to obtain the interlayer spacings. We perform calculations on the unit cells of substrates to obtain their irreducible polarizabilities. The *k*-point sampling in the polarizability calculations is the same as those for the DFT calculations. The dielectric cutoff used for graphene, BLG,

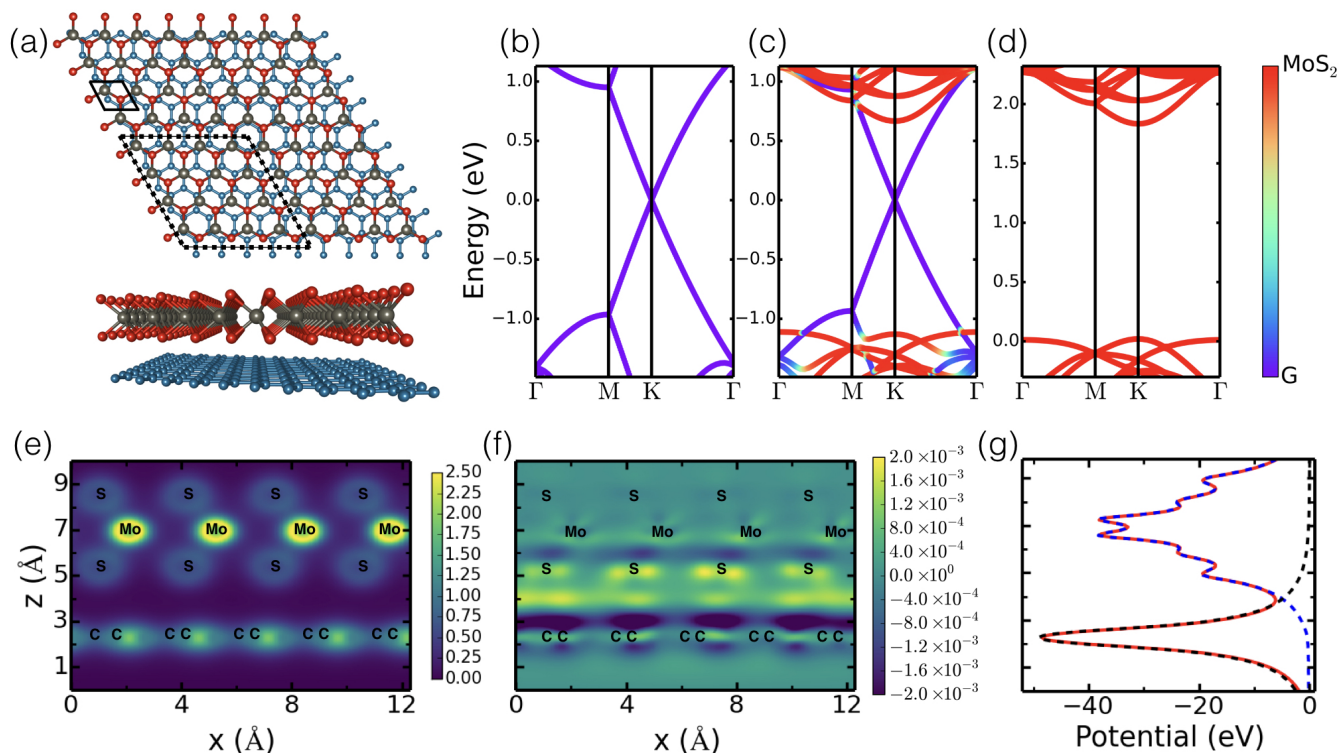


FIG. 1. (a) Single-layer MoS₂ on a graphene substrate, top view and side view. The black solid line marks the unit cell of MoS₂. The dotted line marks the lattice-matched supercell used to perform the DFT calculations. (b)–(d) DFT band structures of free-standing 5 × 5 supercell of graphene, lattice-matched graphene-MoS₂ heterostructure, and free-standing 4 × 4 supercell of MoS₂, respectively. The colors indicate the projected weights of the heterostructure wave functions onto the free-standing layers. (e) The charge density of the MoS₂-graphene heterostructure, in $e/\text{Å}^3$, averaged along one of the in-plane lattice directions. (f) The charge density difference, between the MoS₂-graphene heterostructure and the corresponding free-standing layers. (g) The potential of the MoS₂-graphene heterostructure (red line), the free-standing graphene, and the free-standing MoS₂ layer (blue line).

TLG, and graphite is 10 Ry. For BN and SiO₂, the dielectric cutoff used is 12 and 10 Ry, respectively. The number of unoccupied states for graphene, BLG, TLG, and graphite is 250. For BN and SiO₂, the number of states is 600 and 300, respectively. For metallic substrates, the polarizability at the q point close to the Γ point is computed with a finer k -point sampling of $80 \times 80 \times 1$.

III. EFFECT OF SUBSTRATE SCREENING

We study the interaction between MoS₂ and a substrate at the DFT level by constructing commensurate supercells that accommodate the two materials with a strain of less than 2%. We use a 4 × 4 supercell of MoS₂ and a 5 × 5 supercell of graphene. Figure 1(a) shows MoS₂ on a graphene substrate. A similar geometry is used for the case of MoS₂ on BN since the lattice parameter of BN is close to that of graphene. The BN or graphene layers are strained to attain a commensurate supercell. The relaxed interlayer spacing for the MoS₂-graphene heterostructure is 3.1 Å. Figures 1(b) and 1(d) show the DFT band structure of the 5 × 5 supercell of graphene and the 4 × 4 supercell of MoS₂, respectively. Figure 1(c) shows the band structure of the MoS₂-graphene heterostructure. The DFT wave function of the heterostructure, for a given band and k point, has been projected onto the wave functions of free-standing graphene and free-standing MoS₂. The projected weights are then portrayed using a color map.

Note that the energy of the VBM has been set to zero in these plots. It can be seen that interlayer coupling or hybridization is absent at the VBM and CBM of MoS₂ in the heterostructure. At the DFT level, the band gap of MoS₂ in the presence of graphene is unchanged. This is different from bilayer MoS₂ where the overlap of wave functions of similar energies leads to strong hybridization and a transition of the gap from direct to indirect [76]. Slight hybridization is, however, seen far from the Fermi level, leading to the creation of small gaps in graphene of about 70 meV. These minigaps have been recently observed in MoS₂-graphene heterostructures using angle-resolved photoemission spectroscopy (ARPES) [77,78]. Figure 1(e) plots the charge density of the MoS₂-graphene heterostructure, $\rho^{\text{MG}}(\mathbf{r})$, averaged along one of the in-plane lattice vectors. Figure 1(f) plots the charge density difference, $\rho^{\text{MG}}(\mathbf{r}) - \rho^{\text{M}}(\mathbf{r}) - \rho^{\text{G}}(\mathbf{r})$, in the same manner. In the heterostructure, the electronic charge density within each layer is slightly rearranged, but there is no possibility of charge transfer from one layer to the other due to the sizable energy difference between the graphene Fermi level and the MoS₂ CBM. Our Bader charge analysis further supports the absence of charge transfer. The directionality of the rearrangement of charges, leading to the formation of out-of-plane dipole moments, is explained by the nonuniform potential gradient induced in one layer due to the other [Fig. 1(g)]. At the equilibrium spacing, the potential from one layer is finite and decreasing in the vicinity of the other layer. This gradient acts as an effective

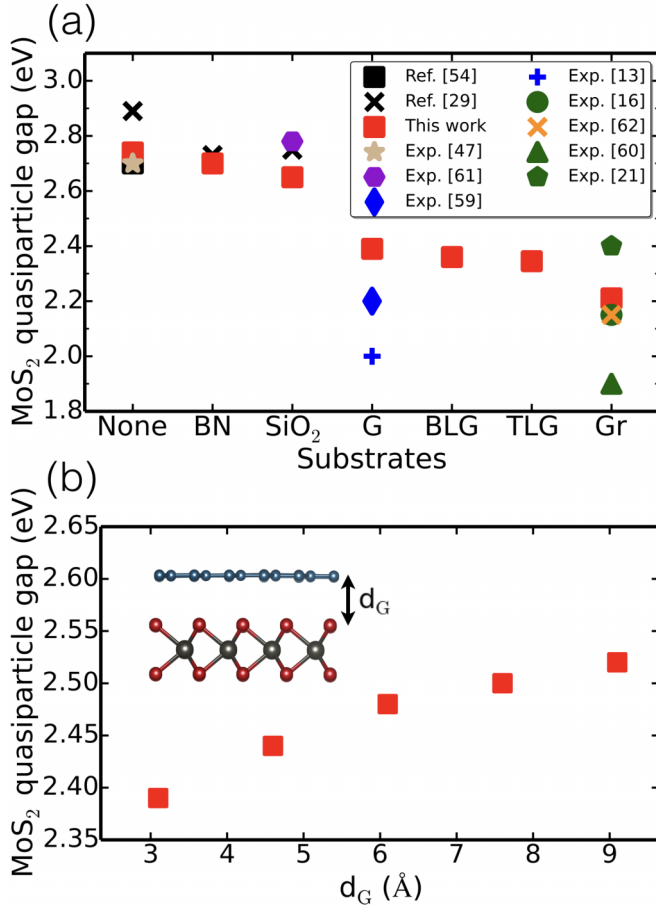


FIG. 2. (a) Quasiparticle band gap of MoS₂, free-standing, and in the presence of monolayer BN, bulk SiO₂, graphene (G), bilayer graphene (BLG), trilayer graphene (TLG), and graphite substrates. Experimental measurements of the quasiparticle gap in these systems are also shown in the plot. (b) Quasiparticle band gap of MoS₂ in the presence of graphene as a function of increasing interlayer spacing d_G .

electric field for the other layer, leading to the rearrangement of electrons.

Performing *GW* calculations on the various supercell geometries is computationally demanding. We instead perform separate unit cell calculations on MoS₂ and the substrates. To take into account the effect of a substrate on MoS₂, we map the in-plane $\vec{q} + \vec{G}$ vectors of the MoS₂ irreducible polarizability $\chi_{\vec{q}+\vec{G}}$ to $\vec{q} + \vec{G}$ vectors of the substrate irreducible polarizability. The substrate polarizability element corresponding to the mapped $\vec{q} + \vec{G}$ vector is then added to the polarizability element of MoS₂ [55,57,58]. Using this method, the band-gap reduction is slightly overestimated for bulk substrates. Figure 2(a) shows the quasiparticle band gap of MoS₂ in the free-standing case and in the presence of BN, SiO₂, graphene (G), bilayer graphene (BLG), trilayer graphene (TLG), and graphite (Gr) substrates. Also marked in the figure are the experimentally measured quasiparticle band gaps of MoS₂ on these substrates. A significant renormalization to the band gap of MoS₂ is captured at the *GW* level, while the gap remains unchanged at the DFT level. This is due to the inclusion of image charge effects at the *GW* level. The

more metallic nature of the substrate, the larger is the band-gap renormalization. A similar trend is observed for molecules on a metal substrate, where DFT fails to predict any renormalization to the molecular levels, while *GW* effectively captures the nonlocal screening due to image charge effects and shows a renormalization, in agreement with experimental findings [79–81]. The renormalization of the MoS₂ quasiparticle band gap in the presence of BN and SiO₂ is 40 and 90 meV, respectively. In the presence of graphene, BLG, TLG, and graphite, the renormalization is 350, 380, 400, and 530 meV, respectively. Our result for the renormalization in the presence of graphene is in good agreement with a recent *GW* calculation on the explicit MoS₂-graphene heterostructure [24]. The value of the quasiparticle band gap measured experimentally is in excellent agreement for the free-standing case and in the presence of a SiO₂ substrate [Fig. 2(a)]. The experimental quasiparticle band gap of MoS₂ measured in the presence of a graphene and graphite substrate, on the other hand, is varied and falls in the range of 1.9–2.4 eV [Fig. 2(a)]. In Fig. 2(a), all the experimental values reported are measured using scanning tunneling spectroscopy, except the one on the SiO₂ substrate, which uses photoluminescence excitation spectroscopy. We additionally study the effect of MoS₂-graphene interlayer spacing on the quasiparticle band gap of MoS₂. We find that the gap is sensitive to the spacing and can be tuned from 2.4 to 2.5 eV [Fig. 2(b)]. We estimate the error in our calculation of the quasiparticle band gap is 100 meV in the case of the 2D substrates and 150 meV in the case of bulk substrates. There exist other factors in the experiment that could lead to a further renormalization of the band gap in MoS₂. These include the effect of carrier-induced plasmons in the system, which have recently been shown to close the gap by up to 150 meV [61,82]. Additional screening from the metallic tip of the scanning tunneling microscope could also further renormalize the band gap [83].

IV. SULFUR VACANCY DEFECT

Figure 3(a) shows the DFT band structure of a 5×5 supercell of MoS₂ with a sulfur vacancy defect. Three defect states are induced in the gap on introducing the vacancy: one filled (indicated by green) bonding state and two degenerate unfilled (indicated by blue) antibonding states. The charge density associated with these defect states is shown in Figs. 3(b) and 3(c). The empty states are localized over a smaller region in the material as compared to the filled state. These defect states are dominantly of the Mo-*d* character [Fig. 3(a)]. We compare the VBM and CBM of the pristine MoS₂ system, and the defect levels with respect to the vacuum level as computed within DFT and *GW*. Figures 4(a) and 4(b) show a schematic of this comparison. We find that the DFT calculated CBM and the *GW* calculated CBM differ by about 0.1 eV, while the respective VBMs are different by 1 eV. Interestingly, the empty defect levels are found to line up. The filled defect level, on the other hand, remains shallow and close to the VBM. It has been shown that the CTLs of bulk systems line up between DFT and *GW* with respect to the average electrostatic potential in the system [53]. Here, we find that the defect levels line up with respect to the vacuum level, while the CTLs do not (Fig. 4).

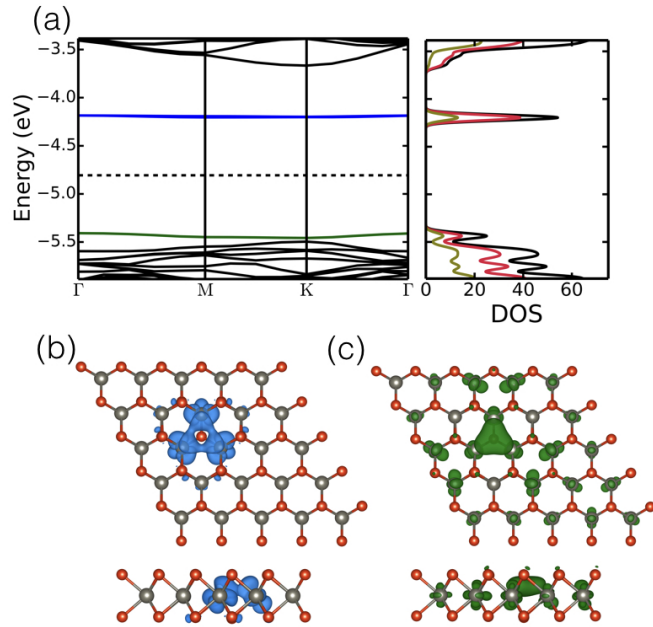


FIG. 3. (a) DFT computed band structure of a sulfur vacancy defect in a 5×5 supercell of MoS₂. Three defect states are induced in the gap. The filled defect level is indicated in green, and the unfilled levels are doubly degenerate and indicated in blue. The black dashed line marks the Fermi level. Partial density of states (DOS) of the 5×5 supercell of MoS₂ with a sulfur vacancy is on the right. The red line shows the Mo-*d* contribution and the green line shows the S-*p* contribution to the total density of states (black). The density of states are in units of states/eV/supercell. (b) and (c) Isosurface of the defect levels induced in the gap of MoS₂. The wave function plotted in blue is the corresponding unfilled defect level in the band structure and the one plotted in green is the filled defect level. The top view as well as the side view are shown.

The formation energy of a sulfur vacancy in charge state q is given by

$$E_q^f[\vec{R}_q](E_F) = \{E_q^{\text{tot}}[\vec{R}_q] + E_q^{\text{corr}}\} - E_{\text{pristine}} + q\{\epsilon_{\text{vbm}}^{\text{pristine}} + E_F - \Delta V_{0/p}\} - \mu_S, \quad (1)$$

where $E_q^{\text{tot}}[\vec{R}_q]$ refers to the total energy of the 5×5 supercell of MoS₂ containing the defect in charge state q . \vec{R}_q refers to the relaxed atom positions in the supercell of the defect system in charge state q . E_q^{corr} is the electrostatic correction term to account for the spurious interaction of the charged defect with its periodic images. This term is zero for the case of the neutral defect. E_{pristine} is the total energy of a pristine supercell of MoS₂ of the same size. The formation energy is a function of the Fermi level with respect to the VBM of the pristine system, $\epsilon_{\text{vbm}}^{\text{pristine}} + E_F$. $\Delta V_{0/p}$ is the potential alignment term found by comparing the electrostatic potential of the neutral defect cell and pristine cell, far from the defect. μ_S is the chemical potential of the sulfur atom removed from the pristine system to form the vacancy defect. This reference can be chosen to simulate sulfur-rich or sulfur-poor ambient conditions. For the sulfur-rich conditions, the chemical potential is chosen from the cyclo-S₈ allotrope of sulfur. For sulfur-poor conditions, the chemical potential is chosen 1.3 eV below the potential at which MoS₂ is reduced to body-centered-cubic (bcc) Mo

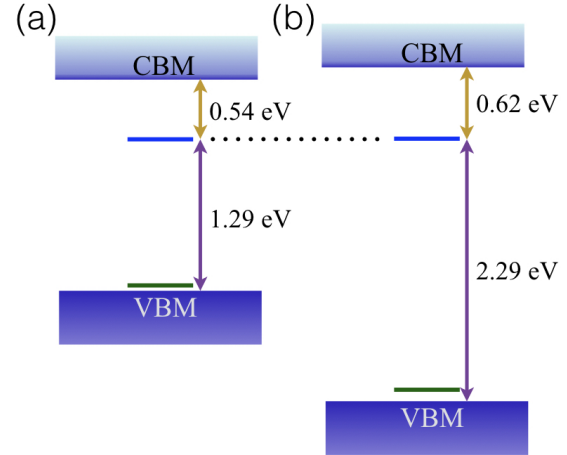


FIG. 4. (a) Schematic of the DFT pristine VBM, pristine CBM, and the defect levels, plotted with respect to the vacuum level. (b) Schematic of the GW pristine VBM, pristine CBM, and the defect levels, plotted with respect to the vacuum level. The dotted line is a guide to the eye, showing that the unfilled defect levels line up between DFT and GW levels of theory.

metal [84,85]. Figures 5(a) and 5(b) plot the DFT computed formation energy of the sulfur vacancy in 0, -1, and +1 charge states as a function of the Fermi level. The Fermi level scans the pristine MoS₂ gap. The formation energy here is determined following Eq. (1) using the DFT computed total energy differences. The electrostatic correction term is determined to be $0.1q^2$ eV, where q is the charge state of the vacancy. The charge transition level, the Fermi level at which the formation energy of one charge state of the defect is equal to that of another, is given by

$$\epsilon^{q/q-1} = E_{q-1}^f[\vec{R}_{q-1}](E_F = 0) - E_q^f[\vec{R}_q](E_F = 0). \quad (2)$$

The only charge transition level stable in the gap at the DFT level is $\epsilon^{0/-1} = 1.6$ eV from the VBM. This is in good agreement with previous calculations [30,38].

Within the DFT+GW formalism, the expression for the charge transition level can be rewritten into two parts: one that involves adding an electron to the system, and the other that takes into account the lattice relaxation effects due to the added electron [52]. The former is evaluated as a quasiparticle excitation at the GW level and the latter is evaluated at the DFT level,

$$\begin{aligned} \epsilon^{q/q-1} &= (E_{q-1}^f[\vec{R}_{q-1}] - E_{q-1}^f[\vec{R}_q]) \\ &\quad + (E_{q-1}^f[\vec{R}_q] - E_q^f[\vec{R}_q]) \\ &= E_{\text{relax}} + E_{\text{QP}}. \end{aligned} \quad (3)$$

For the $\epsilon^{0/-1}$ evaluated using the DFT+GW formalism, we find $E_{\text{QP}} = 2.3$ eV and $E_{\text{relax}} = -0.1$ eV. The charge transition level is hence 2.2 eV above the pristine VBM. For the $\epsilon^{+1/0}$, we find $E_{\text{QP}} = 0.1$ eV and $E_{\text{relax}} = -0.01$ eV, giving the charge transition level ~ 0.1 eV above the VBM. Figures 5(c) and 5(d) show the plot of formation energy with respect to the Fermi level computed using the DFT+GW formalism. Note that we do not add any electrostatic correction terms here since the quasiparticle excitation energies are taken from the neutral system. The $\epsilon^{0/-1}$ computed using hybrid functionals in the

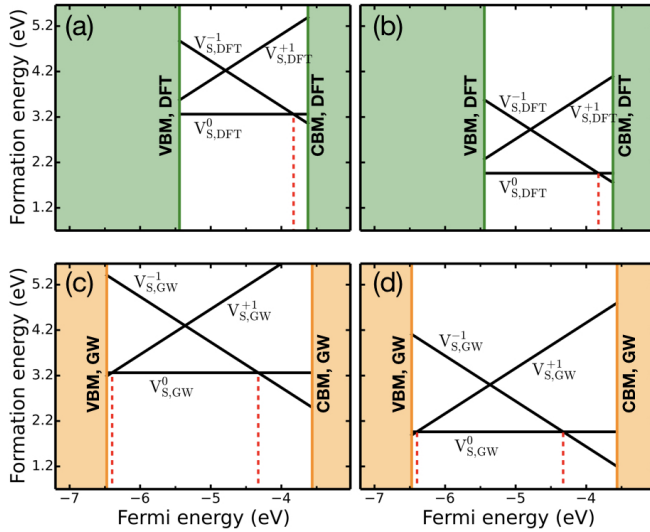


FIG. 5. Formation energy of the sulfur vacancy in different charge states as a function of the Fermi level. The Fermi level is taken to scan the energy range between the pristine VBM and CBM. (a) and (b) Computed at the DFT level, for sulfur-rich and sulfur-poor conditions, respectively. (c) and (d) Computed using the DFT+GW formalism, for sulfur-rich and sulfur-poor conditions, respectively. The charge transition levels that appear in the gap are marked with red dashed lines.

literature are 1.9 eV [30] and 1.6 eV [38] above the VBM. The $\varepsilon^{+1/0}$ computed using hybrid functionals is found to be below the VBM.

V. SUBSTRATE SCREENING EFFECTS ON THE CTLs

The presence of substrates leads to a renormalization of the pristine quasiparticle band gap in MoS₂ [Fig. 2(a)], as well as the term E_{QP} in Eq. (3) for the CTL. We compute the renormalization to E_{QP} from the supercell calculation. The renormalization to the pristine band gap, on the other hand, is taken from the unit cell calculations [Fig. 2(a)]. We also assume that the E_{relax} term is the same in the presence and absence of

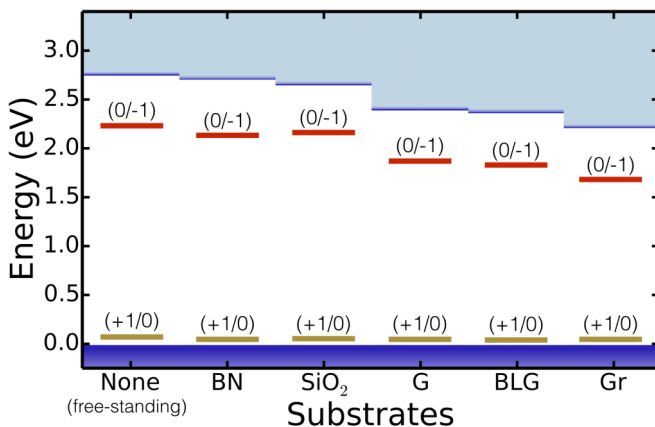


FIG. 6. The $\varepsilon^{+1/0}$ and $\varepsilon^{0/-1}$ charge transition levels of the sulfur vacancy defect computed using the DFT+GW formalism. The levels are shown with respect to the valence band maximum of pristine MoS₂ in the presence of BN, silica, graphene (G), bilayer graphene (BLG), and graphite (Gr) substrates.

substrates. Figure 6 shows the CTLs in the quasiparticle band gap of pristine MoS₂ for the various substrates. The $\varepsilon^{+1/0}$ is pinned close to the VBM, within 100 meV. The defect level involved in this transition is a relatively shallow level with a larger bandwidth [Fig. 3(a)]. The larger bandwidth indicates a slight hybridization with the valence band edge. Hence the effect of substrate screening on this level is similar to that of the VBM. This leads to the pinning of $\varepsilon^{+1/0}$. The $\varepsilon^{0/-1}$, with respect to the VBM, is renormalized by about the same amount as the band gap. The antibonding character of the empty defect states is similar to that of the CBM of the pristine MoS₂ system [39]. The $\varepsilon^{0/-1}$ is thus pinned about 500 meV below the CBM in the presence of substrates as well as in the free-standing configuration (Fig. 6).

VI. CONCLUSION

We have studied the effect of substrate screening on the electronic structure of monolayer MoS₂. The substrates included in our calculations are BN, SiO₂, graphene, bilayer graphene, and graphite. These substrates lead to a significant renormalization of the quasiparticle band gap of MoS₂. In the presence of graphene and graphite substrates, in particular, we find a large reduction of 350 and 530 meV, respectively. These results are in good agreement with recent experimental measurements on these systems [32]. We have also studied the charge transition levels of sulfur vacancy defects in MoS₂ using the DFT+GW formalism. We find two CTLs lying in the pristine quasiparticle band gap of MoS₂, the (+1/0) and the (0/-1) level. The (+1/0) level and (0/-1) level are found 0.07 and 2.14 eV above the pristine VBM, respectively. The stability of the -1 charge state is in good agreement with recent experimental findings. We also compute the CTLs in the presence of substrates. The CTLs show a renormalization similar to that of pristine MoS₂ and *remain* in the pristine band gap of MoS₂. With respect to the VBM, the (0/-1) level is renormalized by the same amount as the gap. The (0/-1) level is thus pinned about 500 meV below the CBM for the free-standing MoS₂ case as well as in the presence of substrates. The (+1/0) level, on the other hand, lies less than 100 meV above the VBM in all the cases. The tuning of the defect levels with a choice of substrate would aid in tuning the binding of hydrogen at the sulfur vacancy sites, which is important to optimize the hydrogen evolution reaction. Charged-defect scattering from the -1 charged sulfur vacancy can be avoided if the Fermi level of the system is below the computed CTL. This could improve the mobility of carriers in MoS₂. The possibility of tuning the CTLs with a choice of substrate need not be restricted to MoS₂. Other transition-metal dichalcogenides and two-dimensional materials could also be expected to show a similar tuning of the defect CTLs.

ACKNOWLEDGMENTS

We thank the Supercomputer Education and Research Centre (SERC) at IISc for providing the computational facilities. Computational facilities from C-DAC's PARAM Yuva II were also used in this work. We thank Felipe H. da Jornada and Diana Y. Qiu for discussions.

- [1] K. F. Mak, C. Lee, J. Hone, J. Shan, and T. F. Heinz, *Phys. Rev. Lett.* **105**, 136805 (2010).
- [2] A. Splendiani, L. Sun, Y. Zhang, T. Li, J. Kim, C.-Y. Chim, G. Galli, and F. Wang, *Nano Lett.* **10**, 1271 (2010).
- [3] Q. H. Wang, K. Kalantar-Zadeh, A. Kis, J. N. Coleman, and M. S. Strano, *Nat. Nanotechnol.* **7**, 699 (2012).
- [4] B. Radisavljevic, A. Radenovic, J. Brivio, V. Giacometti, and A. Kis, *Nat. Nanotechnol.* **6**, 147 (2011).
- [5] K. F. Mak, K. He, J. Shan, and T. F. Heinz, *Nat. Nanotechnol.* **7**, 494 (2012).
- [6] K. Roy, M. Padmanabhan, S. Goswami, T. P. Sai, G. Ramalingam, S. Raghavan, and A. Ghosh, *Nat. Nanotechnol.* **8**, 826 (2013).
- [7] O. Lopez-Sanchez, D. Lembke, M. Kayci, A. Radenovic, and A. Kis, *Nat. Nanotechnol.* **8**, 497 (2013).
- [8] L. Ye, H. Li, Z. Chen, and J. Xu, *ACS Photonics* **3**, 692 (2016).
- [9] H. Li, C. Tsai, A. L. Koh, L. Cai, A. W. Contryman, A. H. Fragapane, J. Zhao, H. S. Han, H. C. Manoharan, F. Abild-Pedersen, J. K. Nørskov, and X. Zheng, *Nat. Mater.* **15**, 48 (2015).
- [10] D. Voiry, M. Salehi, R. Silva, T. Fujita, M. Chen, T. Asefa, V. B. Shenoy, G. Eda, and M. Chhowalla, *Nano Lett.* **13**, 6222 (2013).
- [11] K. Chang, Z. Mei, T. Wang, Q. Kang, S. Ouyang, and J. Ye, *ACS Nano* **8**, 7078 (2014).
- [12] J. Hong, Z. Hu, M. Probert, K. Li, D. Lv, X. Yang, L. Gu, N. Mao, Q. Feng, L. Xie, J. Zhang, D. Wu, Z. Zhang, C. Jin, W. Ji, X. Zhang, J. Yuan, and Z. Zhang, *Nat. Commun.* **6**, 6293 (2015).
- [13] X. Liu, I. Balla, H. Bergeron, G. P. Campbell, M. J. Bedzyk, and M. C. Hersam, *ACS Nano* **10**, 1067 (2015).
- [14] R. Addou, L. Colombo, and R. M. Wallace, *ACS Appl. Mater. Interfaces* **7**, 11921 (2015).
- [15] Y. Lin, X. Ling, L. Yu, S. Huang, A. L. Hsu, Y.-H. Lee, J. Kong, M. S. Dresselhaus, and T. Palacios, *Nano Lett.* **14**, 5569 (2014).
- [16] C. Zhang, A. Johnson, C.-L. Hsu, L.-J. Li, and C.-K. Shih, *Nano Lett.* **14**, 2443 (2014).
- [17] M. K. L. Man, S. Deckoff-Jones, A. Winchester, G. Shi, G. Gupta, A. D. Mohite, S. Kar, E. Kioupakis, S. Talapatra, and K. M. Dani, *Sci. Rep.* **6**, 20890 (2016).
- [18] K. Hsieh, V. Kochat, X. Zhang, Y. Gong, C. S. Tiwary, P. M. Ajayan, and A. Ghosh, *Nano Lett.* **17**, 5452 (2017).
- [19] A. Bruix, J. A. Miwa, N. Hauptmann, D. Wegner, S. Ulstrup, S. S. Grønberg, C. E. Sanders, M. Dendzik, A. Grubišić Čabo, M. Bianchi, J. V. Lauritsen, A. A. Khajetoorians, B. Hammer, and P. Hofmann, *Phys. Rev. B* **93**, 165422 (2016).
- [20] S. Ghatak, S. Mukherjee, M. Jain, D. D. Sarma, and A. Ghosh, *APL Mater.* **2**, 092515 (2014).
- [21] Y. L. Huang, Y. Chen, W. Zhang, S. Y. Quek, C.-H. Chen, L.-J. Li, W.-T. Hsu, W.-H. Chang, Y. J. Zheng, W. Chen, and A. T. S. Wee, *Nat. Commun.* **6**, 6298 (2015).
- [22] Z. Zhang, X. Ji, J. Shi, X. Zhou, S. Zhang, Y. Hou, Y. Qi, Q. Fang, Q. Ji, Y. Zhang, M. Hong, P. Yang, X. Liu, Q. Zhang, L. Liao, C. Jin, Z. Liu, and Y. Zhang, *ACS Nano* **11**, 4328 (2017).
- [23] S. Ulstrup, A. G. Cabo, J. A. Miwa, J. M. Riley, S. S. Grønberg, J. C. Johannsen, C. Cacho, O. Alexander, R. T. Chapman, E. Springate, M. Bianchi, M. Dendzik, J. V. Lauritsen, P. D. C. King, and P. Hofmann, *ACS Nano* **10**, 6315 (2016).
- [24] C. Jin, F. A. Rasmussen, and K. S. Thygesen, *J. Phys. Chem. C* **119**, 19928 (2015).
- [25] K. T. Winther and K. S. Thygesen, *2D Mater.* **4**, 025059 (2017).
- [26] K. Andersen, S. Latini, and K. S. Thygesen, *Nano Lett.* **15**, 4616 (2015).
- [27] J. Ryou, Y.-S. Kim, S. KC, and K. Cho, *Sci. Rep.* **6**, 29184 (2016).
- [28] S. Borghardt, J.-S. Tu, F. Winkler, J. Schubert, W. Zander, K. Leosson, and B. E. Kardynał, *Phys. Rev. Mater.* **1**, 054001 (2017).
- [29] M. Drüppel, T. Deilmann, P. Krüger, and M. Rohlfing, *Nat. Commun.* **8**, 2117 (2017).
- [30] J.-Y. Noh, H. Kim, and Y.-S. Kim, *Phys. Rev. B* **89**, 205417 (2014).
- [31] W. Zhou, X. Zou, S. Najmaei, Z. Liu, Y. Shi, J. Kong, J. Lou, P. M. Ajayan, B. I. Yakobson, and J.-C. Idrobo, *Nano Lett.* **13**, 2615 (2013).
- [32] S. H. Song, M.-K. Joo, M. Neumann, H. Kim, and Y. H. Lee, *Nat. Commun.* **8**, 2121 (2017).
- [33] Y. Ouyang, C. Ling, Q. Chen, Z. Wang, L. Shi, and J. Wang, *Chem. Mater.* **28**, 4390 (2016).
- [34] C. Tsai, F. Abild-Pedersen, and J. K. Nørskov, *Nano Lett.* **14**, 1381 (2014).
- [35] G. Ye, Y. Gong, J. Lin, B. Li, Y. He, S. T. Pantelides, W. Zhou, R. Vajtai, and P. M. Ajayan, *Nano Lett.* **16**, 1097 (2016).
- [36] W. Kohn and L. J. Sham, *Phys. Rev.* **140**, A1133 (1965).
- [37] P. Hohenberg and W. Kohn, *Phys. Rev.* **136**, B864 (1964).
- [38] H.-P. Komsa and A. V. Krasheninnikov, *Phys. Rev. B* **91**, 125304 (2015).
- [39] M. G. Sensoy, D. Vinichenko, W. Chen, C. M. Friend, and E. Kaxiras, *Phys. Rev. B* **95**, 014106 (2017).
- [40] D. Le, T. B. Rawal, and T. S. Rahman, *J. Phys. Chem. C* **118**, 5346 (2014).
- [41] S. KC, R. C. Longo, R. Addou, R. M. Wallace, and K. Cho, *Nanotechnology* **25**, 375703 (2014).
- [42] S. Haldar, H. Vovusha, M. K. Yadav, O. Eriksson, and B. Sanyal, *Phys. Rev. B* **92**, 235408 (2015).
- [43] J. P. Perdew and M. Levy, *Phys. Rev. Lett.* **51**, 1884 (1983).
- [44] J. Heyd, G. E. Scuseria, and M. Ernzerhof, *J. Chem. Phys.* **118**, 8207 (2003).
- [45] J. K. Ellis, M. J. Lucero, and G. E. Scuseria, *Appl. Phys. Lett.* **99**, 261908 (2011).
- [46] S. Bhattacharyya and A. K. Singh, *Phys. Rev. B* **86**, 075454 (2012).
- [47] N. Krane, C. Lotze, J. M. Läger, G. Reecht, and K. J. Franke, *Nano Lett.* **16**, 5163 (2016).
- [48] M. Jain, J. R. Chelikowsky, and S. G. Louie, *Phys. Rev. Lett.* **107**, 216806 (2011).
- [49] P. Rinke, A. Janotti, M. Scheffler, and C. G. Van de Walle, *Phys. Rev. Lett.* **102**, 026402 (2009).
- [50] C. Freysoldt, B. Grabowski, T. Hickel, J. Neugebauer, G. Kresse, A. Janotti, and C. G. Van de Walle, *Rev. Mod. Phys.* **86**, 253 (2014).
- [51] A. Malashevich, M. Jain, and S. G. Louie, *Phys. Rev. B* **89**, 075205 (2014).
- [52] M. Jain, J. R. Chelikowsky, and S. G. Louie, *Phys. Rev. Lett.* **107**, 216803 (2011).
- [53] W. Chen and A. Pasquarello, *J. Phys.: Condens. Matter* **27**, 133202 (2015).
- [54] D. Y. Qiu, F. H. da Jornada, and S. G. Louie, *Phys. Rev. Lett.* **111**, 216805 (2013).
- [55] A. J. Bradley, M. M. Ugeda, F. H. da Jornada, D. Y. Qiu, W. Ruan, Y. Zhang, S. Wickenburg, A. Riss, J. Lu, S.-K. Mo, Z.

- Hussain, Z.-X. Shen, S. G. Louie, and M. F. Crommie, *Nano Lett.* **15**, 2594 (2015).
- [56] D. Y. Qiu, F. H. da Jornada, and S. G. Louie, *Phys. Rev. B* **93**, 235435 (2016).
- [57] M. M. Ugeda, A. J. Bradley, S.-F. Shi, F. H. da Jornada, Y. Zhang, D. Y. Qiu, W. Ruan, S.-K. Mo, Z. Hussain, Z.-X. Shen, F. Wang, S. G. Louie, and M. F. Crommie, *Nat. Mater.* **13**, 1091 (2014).
- [58] D. Y. Qiu, F. H. da Jornada, and S. G. Louie, *Nano Lett.* **17**, 4706 (2017).
- [59] J. Shi, M. Liu, J. Wen, X. Ren, X. Zhou, Q. Ji, D. Ma, Y. Zhang, C. Jin, H. Chen, S. Deng, N. Xu, Z. Liu, and Y. Zhang, *Adv. Mater.* **27**, 7086 (2015).
- [60] C.-I. Lu, C. J. Butler, J.-K. Huang, C.-R. Hsing, H.-H. Yang, Y.-H. Chu, C.-H. Luo, Y.-C. Sun, S.-H. Hsu, K.-H. O. Yang, C.-M. Wei, L.-J. Li, and M.-T. Lin, *Appl. Phys. Lett.* **106**, 181904 (2015).
- [61] K. Yao, A. Yan, S. Kahn, A. Suslu, Y. Liang, E. S. Barnard, S. Tongay, A. Zettl, N. J. Borys, and P. J. Schuck, *Phys. Rev. Lett.* **119**, 087401 (2017).
- [62] M.-H. Chiu, C. Zhang, H.-W. Shiu, C.-P. Chuu, C.-H. Chen, C.-Y. S. Chang, C.-H. Chen, M.-Y. Chou, C.-K. Shih, and L.-J. Li, *Nat. Commun.* **6**, 7666 (2015).
- [63] P. Giannozzi, S. Baroni, N. Bonini, M. Calandra, R. Car, C. Cavazzoni, D. Ceresoli, G. L. Chiarotti, M. Cococcioni, I. Dabo, A. D. Corso, S. de Gironcoli, S. Fabris, G. Fratesi, R. Gebauer, U. Gerstmann, C. Gougoussis, A. Kokalj, M. Lazzeri, L. Martin-Samos *et al.*, *J. Phys.: Condens. Matter* **21**, 395502 (2009).
- [64] M. H. Naik and M. Jain, *Comput. Phys. Commun.* **226**, 114 (2018).
- [65] J. Deslippe, G. Samsonidze, D. A. Strubbe, M. Jain, M. L. Cohen, and S. G. Louie, *Comput. Phys. Commun.* **183**, 1269 (2012).
- [66] M. Rohlfing and S. G. Louie, *Phys. Rev. B* **62**, 4927 (2000).
- [67] M. S. Hybertsen and S. G. Louie, *Phys. Rev. B* **34**, 5390 (1986).
- [68] D. Y. Qiu, F. H. da Jornada, and S. G. Louie, *Phys. Rev. Lett.* **115**, 119901(E) (2015).
- [69] G. Samsonidze, M. Jain, J. Deslippe, M. L. Cohen, and S. G. Louie, *Phys. Rev. Lett.* **107**, 186404 (2011).
- [70] A. Stathopoulos and J. R. McCombs, *ACM Trans. Math. Software* **37**, 21 (2010).
- [71] L. Wu, E. Romero, and A. Stathopoulos, [arXiv:1607.01404](https://arxiv.org/abs/1607.01404).
- [72] L. S. Blackford, J. Choi, A. Cleary, E. D’Azevedo, J. Demmel, I. Dhillon, J. Dongarra, S. Hammarling, G. Henry, A. Petitet, K. Stanley, D. Walker, and R. C. Whaley, *ScaLAPACK Users’ Guide* (Society for Industrial and Applied Mathematics, Philadelphia, PA, 1997).
- [73] J. Deslippe, G. Samsonidze, M. Jain, M. L. Cohen, and S. G. Louie, *Phys. Rev. B* **87**, 165124 (2013).
- [74] S. Ismail-Beigi, *Phys. Rev. B* **73**, 233103 (2006).
- [75] S. Grimme, *J. Comput. Chem.* **27**, 1787 (2006).
- [76] M. H. Naik and M. Jain, *Phys. Rev. B* **95**, 165125 (2017).
- [77] H. Coy Diaz, J. Avila, C. Chen, R. Addou, M. C. Asensio, and M. Batzill, *Nano Lett.* **15**, 1135 (2015).
- [78] D. Pierucci, H. Henck, J. Avila, A. Balan, C. H. Naylor, G. Patriarche, Y. J. Dappe, M. G. Silly, F. Sirotti, A. T. C. Johnson, M. C. Asensio, and A. Ouerghi, *Nano Lett.* **16**, 4054 (2016).
- [79] M. Rohlfing, *Phys. Rev. Lett.* **108**, 087402 (2012).
- [80] J. B. Neaton, M. S. Hybertsen, and S. G. Louie, *Phys. Rev. Lett.* **97**, 216405 (2006).
- [81] K. S. Thygesen and A. Rubio, *Phys. Rev. Lett.* **102**, 046802 (2009).
- [82] Y. Liang and L. Yang, *Phys. Rev. Lett.* **114**, 063001 (2015).
- [83] G. Samsonidze, M. L. Cohen, and S. G. Louie, *Comput. Mater. Sci.* **91**, 187 (2014).
- [84] H. Schweiger, P. Raybaud, G. Kresse, and H. Toulhoat, *J. Catal.* **207**, 76 (2002).
- [85] M. V. Bollinger, K. W. Jacobsen, and J. K. Nørskov, *Phys. Rev. B* **67**, 085410 (2003).